



# Holocene environmental changes in the Horqin desert revealed by OSL dating and $\delta^{13}\text{C}$ analyses of paleosols



Licheng Guo <sup>a, b, \*</sup>, Shangfa Xiong <sup>a</sup>, Ping Yang <sup>c</sup>, Wei Ye <sup>c</sup>, Guiyun Jin <sup>d</sup>, Wenwan Wu <sup>d</sup>, Hua Zhao <sup>e</sup>

<sup>a</sup> Key Laboratory of Cenozoic Geology and Environment, Institute of Geology and Geophysics, Chinese Academy of Sciences, Beijing, 100029, China

<sup>b</sup> University of Chinese Academy of Sciences, Beijing, 100049, China

<sup>c</sup> College of Geography and Environmental Sciences, Zhejiang Normal University, Jinhua, 321004, China

<sup>d</sup> Department of Archaeology, Institute of Cultural Heritage, Shandong University, Jinan, 250100, China

<sup>e</sup> Institute of Hydrogeology and Environmental Geology, Chinese Academy of Geological Sciences, Shijiazhuang, 050061, China

## ARTICLE INFO

### Article history:

Received 1 March 2016

Received in revised form

13 March 2017

Accepted 20 June 2017

Available online 1 July 2017

### Keywords:

Horqin desert

Holocene

East Asian summer monsoon rainfall belt

OSL dating

C<sub>4</sub> plants

## ABSTRACT

The Horqin desert in northeastern China is located on the climatically-sensitive margin of the East Asian summer monsoon front and the paleosols in the desert potentially provide a record of environmental changes in the region. During the last two decades several paleoenvironmental studies have increased our knowledge of past shifts in the desert-grassland border in the deserts of northeastern China. However, studies of Holocene vegetation changes with high-quality age data are scarce. Here, we present the results of optically stimulated luminescence dating and analyses of magnetic susceptibility, total organic carbon and the stable carbon isotope composition of organic matter, and inferred C<sub>4</sub> biomass, of the paleosol sequences of the Tuquan and Mutougou sections in the Horqin desert and utilize them to document Holocene environmental changes in the region. The results reveal that the East Asian summer monsoon precipitation gradually increased and previously unstable dunes were semi-stabilized from ~11 to 9 ka. The semiarid conditions were then replaced by the more humid environment of the Holocene climatic optimum from ~9 to 5 ka. During the Holocene climatic optimum, the paleosols in the Tuquan and Mutougou sections developed, and the percentage of C<sub>4</sub> plants increased and the dunes in the Horqin desert were extensively stabilized. Subsequently, alternation of eolian sand mobilization and paleosol development occurred, indicating that the environment became cold and dry, with temporary wet and warm stages. Estimates of C<sub>4</sub> biomass from the two sections demonstrate that the favorable growing conditions for C<sub>4</sub> plants extended to at least 45°N in North China during the Holocene. We conclude that Holocene environmental changes in the Horqin desert were controlled by movements of the East Asian summer monsoon rainfall belt on a millennial time scale, and that human activity also played a significant role in environmental change during the late Holocene.

© 2017 Elsevier Ltd and INQUA. All rights reserved.

## 1. Introduction

The East Asian summer monsoon (EASM) is one of the major components of the global climate system and its variability significantly influences ecological and social systems in the Asian monsoonal area, particularly on the margin of the EASM front, via its effects on the hydrological system (Yang et al., 2015a) and vegetation distribution (Xiao et al., 2004; Jiang et al., 2006),

especially the position of the desert-grassland border (e.g. Li et al., 2014; Xu et al., 2015). Thus the environment in North China, on the margin of the EASM region, is sensitive to monsoonal changes and is prone to extensive and dramatic ecosystem shifts (Yang et al., 2015a). Consequently, study of the deserts in North China is potentially important for the simulation of paleoclimatic fluctuations in the boundary zone of the EASM and for global climatic models, for improving our understanding of the relationship between past climate and changes in a dryland environment, and for predicting future climate changes in the drylands under a global warming scenario.

The amount of EASM precipitation exerts a major control on

\* Corresponding author. Institute of Geology and Geophysics, Chinese Academy of Sciences, 19 BeiTuChengXi Road, Chaoyang District, Beijing, 100029, China.

E-mail address: [guolicheng05@mail.iggcas.ac.cn](mailto:guolicheng05@mail.iggcas.ac.cn) (L. Guo).

vegetation distribution and dune activity in the Horqin desert. A steppe environment is characteristic during intervals of relatively warm and wet climate, together with the development of paleosols (Qiu et al., 1992; Dong et al., 1994); and conversely, desert environments with active dunes develop during intervals of dry and cold climate (Zhao et al., 2007). Studies of the paleosols in this desert region are potentially able to document environmental changes associated with movements of the EASM front.

Environmental changes in the Horqin desert during the Holocene have been extensively studied during the last two decades. Results from more than ten sections in the western plain of northeastern China suggest that the paleosols were formed during the following intervals: 11–7 ka, 5.5–4.5 ka, 3.5–2.8 ka, and 1.4–1 ka, and that these intervals were linked with movements of the EASM (Qiu et al., 1992). Dong et al. (1994) concluded that seven episodes of dune stabilization occurred in the southern Horqin desert during the Holocene, in response to global climate changes. Another study in the southeastern Horqin desert (Zhao et al., 2007) indicated that Holocene dune activity was characterized by four stages: sand dune mobilization (before 10 ka), dune semi-stabilization (10–7.5 ka), dune stabilization and development of chernozem soils (7.5–2.0 ka), and partial re-mobilization of dunes (~2.0 ka onwards). Results of investigations of an increasing number of sections, described online in Yi et al. (2013) and in Yang et al. (2010, 2012), support the view that the Horqin desert experienced four stages of dune evolution (Zhao et al., 2007); and that Holocene environmental changes in the desert can be regarded as responses to variations in Asian monsoon and effective moisture on a millennial time scale (Mason et al., 2009; Yang et al., 2012; Yi et al., 2013). However, the timing of the changes is poorly constrained and the conclusions are sometimes contradictory. Consequently, this raises the possibility of multiple causes of environmental change in the desert, including both climate change since the Pleistocene (Wang et al., 2008; Yang et al., 2012) and human activity during the historical period (Ren, 1999; Hu et al., 2002; Ren et al., 2004; Yang et al., 2012). Another important issue is that reliable records of Holocene vegetation changes in the Horqin desert are limited (Lu et al., 2012). The only examples are the work of Lu et al. (2012), who used the stable carbon isotope composition of organic matter ( $\delta^{13}\text{C}_{\text{org}}$ ) of sediments to reconstruct the late Quaternary vegetation history, and of Yang et al. (2012) who analyzed pollen assemblages for the interval ~4–2 ka in the ADQ section in the Horqin desert. However, they did not discuss the Holocene vegetation history, and thus it is clear that more work with reliable Holocene vegetation records is needed in this area.

The work of An et al. (2005) indicated that in the drylands of China  $\text{C}_4$  biomass increases with increasing summer precipitation ( $R^2 = 0.70$ ) (An et al., 2005); and that of Wang et al. (2013) indicated that in North China the  $\text{C}_4$  biomass increases with increasing mean annual temperature (MAT) ( $R^2 = 0.35$ ) along the 400 mm isoline of the mean annual precipitation (MAP). More recently, Yang et al. (2015b) demonstrated that spatiotemporal changes in  $\text{C}_4$  plants in the Chinese Loess Plateau are closely related to the movement of the EASM rainfall belt. In general, high summer precipitation favors the growth of  $\text{C}_4$  plants and produces strong pedogenesis (Lu et al., 2012, 2013). Consequently, paleosols develop and dunes are extensively fixed within desert areas. In addition, the magnetic susceptibility ( $\chi$ ) of loess-paleosol sequences is widely used as a proxy of EASM strength (Xiong et al., 2002) due to the fact that strong pedogenesis (Maher and Thompson, 1995) and decomposition of plants (Meng et al., 1997) can enhance the  $\chi$  of paleosols. Based on these results, we infer that the  $\chi$  and  $\text{C}_4$  biomass of paleosols in the study area can serve as two robust proxies for reconstructing environmental changes in deserts.

The present paper is a further exploration of the Holocene

history of the Horqin desert, with the aim of improving our understanding of vegetation and climate changes. Specifically, we present the results of optically stimulated luminescence (OSL) dating of Holocene paleosol sequences of the Tuquan (TQ) and Mutougou (MTG) sections (Fig. 1), together with the results of analyses of  $\chi$  and total organic carbon (TOC) and  $\delta^{13}\text{C}_{\text{org}}$  and changes in  $\text{C}_4$  biomass.

## 2. Regional setting

The Horqin desert (42°40′–45°15′N, 118°30′–124°30′E, and 120–800 m a.s.l.), with a surface area of about 50,440 km<sup>2</sup>, is located in the Xiliao river drainage area in northeastern China, about 400 km northeast of Beijing (Fig. 1). Situated in the margin of the EASM front (Fig. 1), the current climate is semi-arid, dominated by the EASM. The Horqin desert receives about 70% of MAP during the summer, and MAT is 3–7 °C. MAP ranges from 500 mm in the southeast to 350 mm in the northwest (Hu, 1989), and the mean annual potential evaporation is 1500–2500 mm (Ren et al., 2004). The natural vegetation in this desert is temperate steppe (Ren et al., 1985); however, it is frequently replaced by desert-steppe vegetation due to over-grazing and over-cultivation (Ren et al., 2004).

## 3. Material and methods

### 3.1. Stratigraphy and sampling

The TQ (45°11.070′N, 121°33.760′E) and MTG (42°31.402′N, 118°51.843′E) sections, exposed in outcrops and situated on a river terrace (Fig. S1), are located in the northern and southwestern parts of the Horqin desert (Fig. 1), respectively. The lithology of the TQ section (Fig. 2) consists of two main units: eolian sands (5.0–5.2 m, 3.7–3.9 m and 2.8–2.9 m) and sandy paleosols (3.9–5.0 m, 2.9–3.7 m, 1.3–2.8 m and 0–1.3 m). The shallowest sandy paleosol layer is mixed with modern soil. The lithology of the MTG section (Fig. 3) can be divided into three units: the lowermost unit (5.4–5.0 m) consists of a coarse loess layer; the middle unit (5.0–0.3 m) is a paleosol layer with white carbonate precipitates from 2.0 to 0.3 m and root channels from 5.0 to 2.0 m; and the uppermost unit (0–0.3 m) consists of grey-yellow sand.

Eleven samples for OSL dating (Figs. 2 and 3) were collected from the two freshly dug sections, the outer 0.5 m of which was removed, by hammering aluminum tubes into the cleaned vertical sections. After removal they were sealed in black plastic bags to minimize light exposure and moisture loss (Zhao et al., 2007). In addition, a total of 106 samples were taken at 10–20 cm intervals from the two sections for carbon isotope analysis of bulk organic matter and magnetic susceptibility measurements.

### 3.2. OSL dating

The OSL samples were prepared and measured at the Institute of Earth Environments, Chinese Academy of Sciences. Samples for dating were taken from the central 5 cm interval of the sediment core in the sample tubes and were then prepared under subdued red light conditions using the procedure of Kang et al. (2015).

The sample used to determine the equivalent dose was first treated with 30%  $\text{H}_2\text{O}_2$  to remove organic material and then with 30% HCl to remove inorganic carbonate, followed by settling and sieving to isolate the 4–11 and 90–125  $\mu\text{m}$  grain-size fractions for MTG and TQ sections, respectively (Guo et al., 2016). The applicability of the fractions for OSL dating was assessed on the basis of particle size and the natural alpha, beta, gamma and cosmic radioactivity (Aitken, 1998). Subsequently, the coarse-grained (90–125  $\mu\text{m}$ ) quartz was separated by heavy liquid flotation

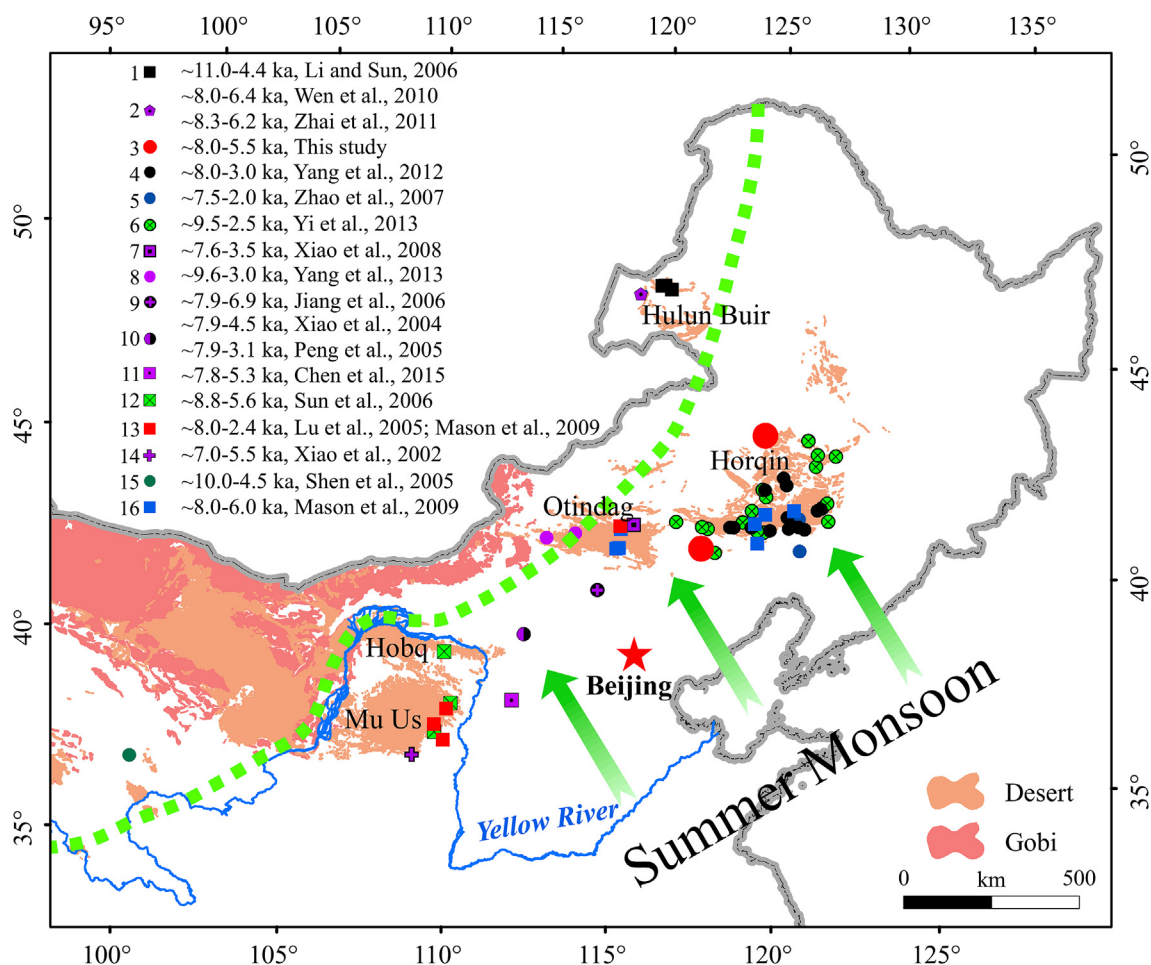


**Fig. 1.** Location of various sites in North China used to infer the timing (shown in ka) of maximum Holocene EASM precipitation along the margin of the East Asian Summer Monsoon front (green dashed line). The distribution of deserts is also shown (This data set is provided by Environmental and Ecological Science Data Center for West China, National Natural Science Foundation of China, <http://westdc.westgis.ac.cn>). Paleosol sites include the TQ and MTG sections (3 solid red circles; this work) in the Horqin desert; the results from other sites in the Horqin desert are described in 4–6 and 16 (exact locations of the sites are also shown); Hulun Buir desert (1); Otindag desert (8, 13 and 16); Mu Us desert (12 and 13); Hobq desert (12); and Jiangbian (14). Lake sites include Hulun Lake (2); Dali Lake (7); Bayanchagan Lake (9); Daihai Lake (10); Gonghai Lake (11); and Qinghai Lake (15). (For interpretation of the references to colour in this figure legend, the reader is referred to the web version of this article.)

(sodium polytungstate), and the fine-grained (4–11  $\mu\text{m}$ ) quartz was extracted by treatment with 30% HF for about one week. The coarse-grained quartz was rinsed, and then etched with 40% HF for 60 mins to remove feldspar minerals and the alpha-irradiated surface layer of the quartz grains, followed by HCl rinsing to remove insoluble fluorides. Finally, the purified quartz was dried at 45  $^{\circ}\text{C}$  and mounted on steel discs using ethanol and silicon-based adhesive for fine-grained and coarse-grained quartz, respectively. The purity of quartz extracts was tested by infrared stimulated luminescence.

OSL measurements were performed using an automated Daybreak 2200 OSL reader system. Equivalent doses of each sample were measured using the single-aliquot regenerative-dose (SAR) protocol (Wintle and Murray, 2006). The environmental dose rate was measured using the methods described in Kang et al. (2015). An average water content of  $10 \pm 5\%$  is the average wetness during the entire burial time on the basis of works in similar environmental settings (Zhao et al., 2007). The cosmic dose rates were also taken into account (Prescott and Hutton, 1994).

### 3.3. $\delta^{13}\text{C}$ analysis of bulk organic matter and magnetic susceptibility measurements

The samples ( $\sim 3$  g), which were screened for modern rootlets,

were digested in 1 M HCl at  $\sim 25$   $^{\circ}\text{C}$  for 24 h to remove inorganic carbonate and were then washed to a near-neutral pH condition (the pH ranged from 5 to 7) with distilled water and oven-dried at 50  $^{\circ}\text{C}$ . The dried samples ( $\sim 20$  mg) were combusted for 4 h at 850  $^{\circ}\text{C}$  in evacuated sealed quartz tubes in the presence of silver foil and cupric oxide. The carbon isotopic composition of  $\text{CO}_2$  was measured using a MAT-253 gas mass spectrometer with a dual inlet system at the Institute of Geology and Geophysics, Chinese Academy of Sciences; the total organic carbon content (TOC) of the samples was determined simultaneously. The TOC is exclusively derived from terrestrial higher plants because hydrophytes would not be able to survive given the high mean annual potential evaporation (1500–2500 mm) in the desert. Thus the  $\delta^{13}\text{C}_{\text{org}}$  values obtained relate mainly to the  $\text{C}_4$  biomass (Rao et al., 2008; Lu et al., 2012). Magnetic susceptibility ( $\chi$ ) measurements were made on air-dried samples using a Bartington Instruments MS3 magnetic susceptibility meter at a frequency of 0.47 kHz.

### 3.4. Vegetation reconstruction

A previous study (Wang et al., 2013) demonstrated that along the 400 mm isoline of MAP in North China, the  $\delta^{13}\text{C}$  values of  $\text{C}_3$  plants ( $\delta^{13}\text{C}_{\text{C}_3}$ ) range from  $-24.32\%$  to  $-31.26\%$ , with a mean of  $-27.80\%$ ; and those of  $\text{C}_4$  plants ( $\delta^{13}\text{C}_{\text{C}_4}$ ) range from  $-10.46\%$

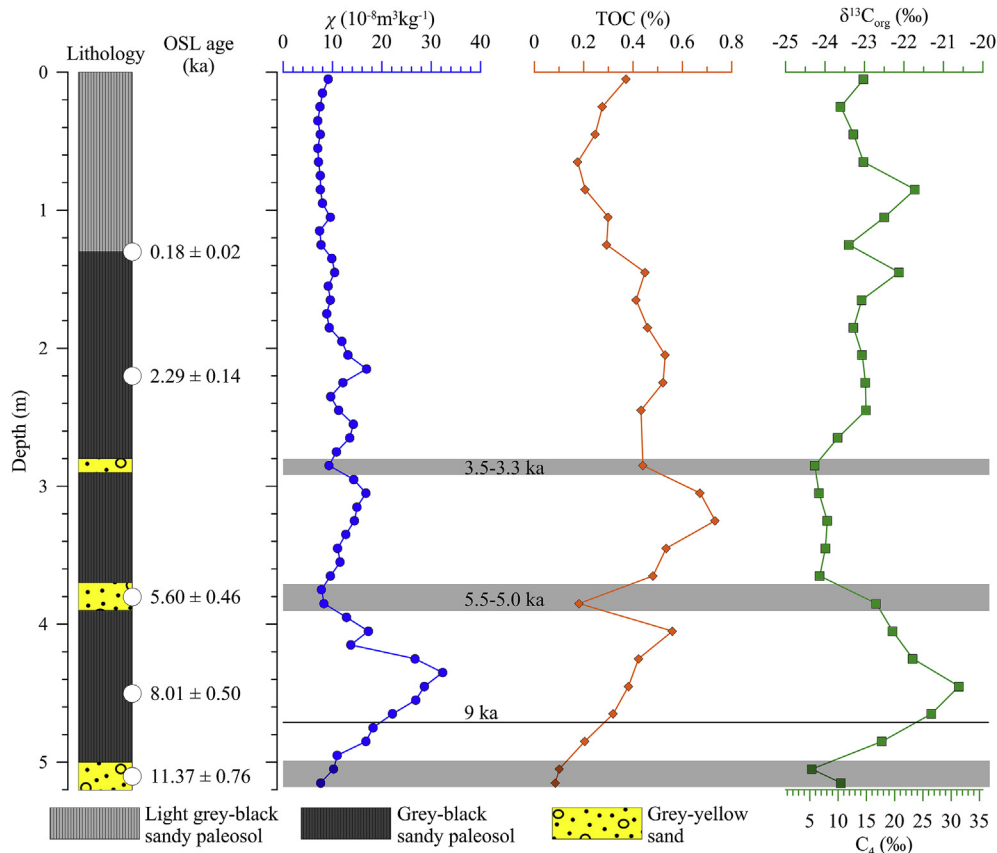


**Fig. 2.** Stratigraphy, sampling position (white circles), OSL ages and changes in paleoenvironmental proxies for the TQ section. Eolian sand is shown by the light grey shading.

to  $-22.31\%$ , with a mean of  $-13.48\%$ . Considering the major effects of the carbon isotopic composition of atmospheric  $\text{CO}_2$  together with organic matter degradation, but assuming that the climatic conditions during the Holocene changed only slightly and thus ignoring corrections for precipitation and temperature, the transformation from  $\delta^{13}\text{C}_{\text{org}}$  to  $\text{C}_4$  biomass in the TQ and MTG sections is based on the method described in Yang et al. (2015b) by applying the measured  $\delta^{13}\text{C}_{\text{org}}$  values to an isotope mass-balance equation:  $\text{C}_4 (\%) = [(\delta^{13}\text{C}_{\text{org}} - \delta^{13}\text{C}_{\text{C}_3}) / (\delta^{13}\text{C}_{\text{C}_4} - \delta^{13}\text{C}_{\text{C}_3})] \times 100$ . We ignored the slight effect of changes in atmospheric  $\text{CO}_2$  concentration during the Holocene (Wang and Feng, 2012). Thus, the ignorable uncertainty of the vegetation reconstruction has a faint effect on the interpretation of the  $\text{C}_4$  biomass.

## 4. Results

### 4.1. Chronology

The OSL ages for the TQ and MTG sections are presented in Table 1 and illustrated in Fig. S2. The equivalent dose determination of the fine-grained (4–11  $\mu\text{m}$ ) and coarse-grained (90–125  $\mu\text{m}$ ) quartz show similar luminescence characteristics (Fig. S2). OSL intensity decays during the first few seconds, and the growth curve can be well fitted using a single saturating exponential plus constant function; in addition, the equivalent dose distribution exhibits a tight normal distribution. These characteristics suggest that the samples were well bleached prior to deposition and can be used to determinate the equivalent dose.

Interpretation of the OSL ages of paleosols is complex (Lu et al., 2011; Yang et al., 2012) because of the effects of eolian erosion and

bioturbation. However, the weaker dune mobility on the perimeter of the Horqin desert, evidenced by the presence of only two thin layers of eolian sand in the TQ section, implies that the stratigraphic sequences from the two sites are only slightly affected by eolian erosion. Thus, we infer that paleosol formation began at  $\sim 10$  ka and ended at  $\sim 1$  ka, and the eolian sands accumulated and/or soil formation was limited during two intervals, from  $\sim 5.5$  to 5 ka and  $\sim 3.5$ –3.3 ka.

### 4.2. Changes in paleoenvironmental proxies during the Holocene

Changes in  $\chi$ , TOC,  $\delta^{13}\text{C}_{\text{org}}$  and  $\text{C}_4$  biomass are plotted in Figs. 2 and 3. There are significant differences between the values of  $\chi$ , TOC and  $\text{C}_4$  biomass in the two sections. The  $\chi$  and TOC values for the TQ section are much lower than those for the MTG section, presumably because of much weaker pedogenesis (Maher and Thompson, 1995) and a lower organic content (Meng et al., 1997). The values of  $\text{C}_4$  biomass in the MTG section are higher than those of the TQ section. The TOC values of the TQ section average around 0.4%; however, they exhibit an overall increasing trend in both sections. In the TQ section,  $\chi$ ,  $\delta^{13}\text{C}_{\text{org}}$  and  $\text{C}_4$  biomass exhibit relatively high values from  $\sim 9$  to 5 ka. From  $\sim 5$  to 1 ka and  $\sim 11$ –9 ka, the values of  $\chi$ ,  $\delta^{13}\text{C}_{\text{org}}$  and  $\text{C}_4$  biomass are low and fluctuating. However, the values of  $\chi$ ,  $\delta^{13}\text{C}_{\text{org}}$  and  $\text{C}_4$  biomass from the MTG section increase gradually from  $\sim 11$  to 5 ka, reach their maxima at  $\sim 6$  ka, and tend to decrease with fluctuations from  $\sim 5$  to 1 ka. Consequently, the  $\chi$  and  $\delta^{13}\text{C}_{\text{org}}$  and  $\text{C}_4$  biomass records can be divided into three stages, from  $\sim 11$  to 9 ka, from  $\sim 9$  to 5 ka and from  $\sim 5$  to 1 ka. During the interval  $\sim 11$ –9 ka,  $\chi$ ,  $\delta^{13}\text{C}_{\text{org}}$  and  $\text{C}_4$  biomass exhibit relatively low values overall; however, they increase slightly within

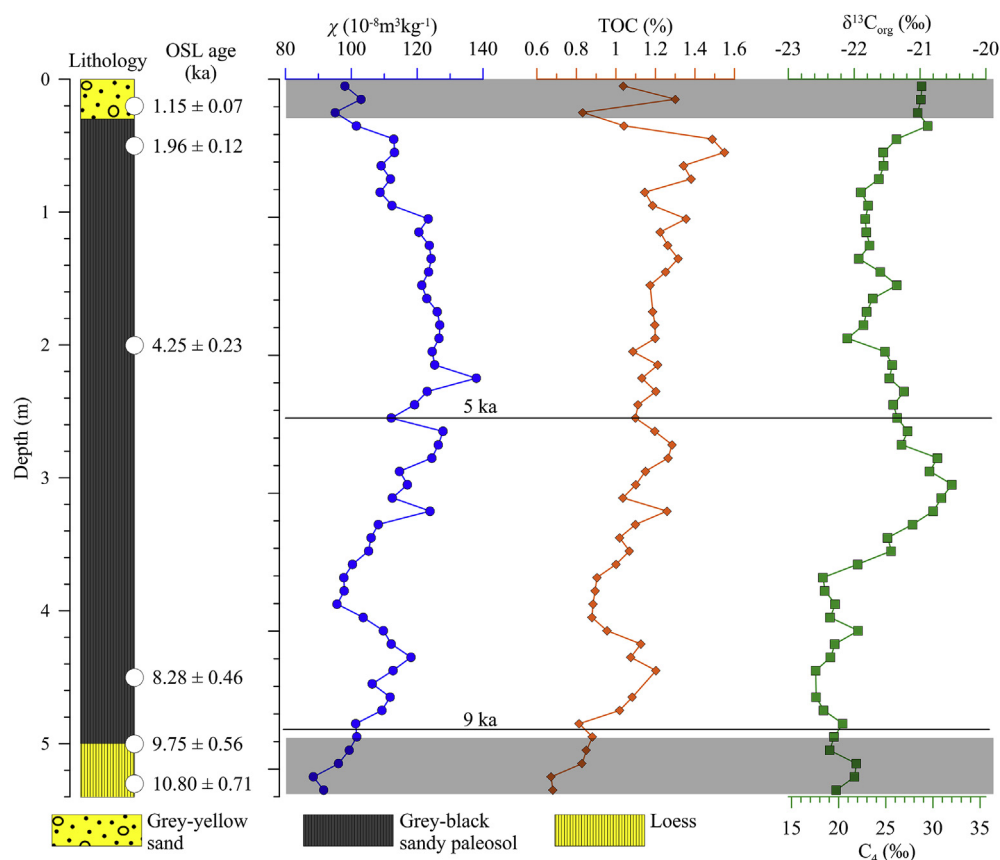


**Fig. 3.** Stratigraphy, sampling position (white circles), OSL ages and changes in paleoenvironmental proxies for the MTG section. Eolian sand and loess are shown by the light grey shading.

**Table 1**

Results of OSL dating of samples from the TQ and MTG sections in the Horqin desert.

Sample code	Depth (m)	U (ppm)	Th (ppm)	K (%)	Equivalent doses (Gy)	Dose rate (Gy/ka)	Water content (%)	OSL age (ka)
TQ-OSL-02	1.30	0.55	2.51	1.73	0.36 ± 0.03	1.99 ± 0.10	10 ± 5	0.18 ± 0.02
TQ-OSL-03	2.20	0.69	3.32	2.09	5.43 ± 0.16	2.37 ± 0.13	10 ± 5	2.29 ± 0.14
TQ-OSL-05	3.80	0.54	2.39	1.84	11.34 ± 0.68	2.02 ± 0.11	10 ± 5	5.60 ± 0.46
TQ-OSL-06	4.50	0.84	3.98	2.14	19.62 ± 0.63	2.45 ± 0.13	10 ± 5	8.01 ± 0.50
TQ-OSL-07	5.10	0.62	2.74	2.03	25.16 ± 0.97	2.21 ± 0.12	10 ± 5	11.37 ± 0.76
MTG-OSL-01	0.20	1.85	9.54	2.26	4.32 ± 0.10	3.74 ± 0.20	10 ± 5	1.15 ± 0.07
MTG-OSL-02	0.50	1.73	10.60	2.21	6.34 ± 0.16	3.23 ± 0.17	10 ± 5	1.96 ± 0.12
MTG-OSL-04	2.00	1.83	10.60	2.23	15.87 ± 0.12	3.73 ± 0.20	10 ± 5	4.25 ± 0.23
MTG-OSL-06	4.50	1.74	10.33	2.32	30.77 ± 0.19	3.72 ± 0.20	10 ± 5	8.28 ± 0.46
MTG-OSL-07	5.00	1.75	10.10	2.30	35.80 ± 0.65	3.67 ± 0.20	10 ± 5	9.75 ± 0.56
MTG-OSL-08	5.30	1.83	10.46	2.32	40.45 ± 1.48	3.75 ± 0.21	10 ± 5	10.80 ± 0.71

a narrow range.  $\chi$ ,  $\delta^{13}\text{C}_{\text{org}}$  and  $\text{C}_4$  biomass exhibit high values from ~9 ka to ~5 ka, and reach a maximum from ~8 to 5.5 ka. Subsequently, the records exhibit lower values but with fluctuations from ~5 to 1 ka.

## 5. Discussion

### 5.1. Inferred environmental changes in the Horqin desert during the Holocene

Intervals of paleosol formation in the Horqin desert and adjacent deserts (Fig. 4) indicate that at these intervals active dunes were stabilized and the vegetation coverage increased significantly (Qiu et al., 1992; Dong et al., 1994). In the MTG and TQ sections,

prior to ~9 ka, the values of  $\chi$  and  $\text{C}_4$  biomass were low but increasing, and paleosol formation began at ~10 ka. The records imply that the active dunes were semi-stabilized with EASM precipitation gradually increasing from ~11 to 9 ka.

From ~9 to 5 ka, the high  $\chi$  and  $\delta^{13}\text{C}_{\text{org}}$  and  $\text{C}_4$  biomass values indicate a relatively wet climate with intensified monsoonal precipitation, with maximum precipitation occurring from ~8 to 5.5 ka. These findings demonstrate that within the study region the Holocene climatic optimum occurred from ~9 to 5 ka and culminated from ~8 to 5.5 ka; and thus that the maximum EASM precipitation during the Holocene significantly lagged the summer insolation peak which occurred at ~11 ka (Laskar et al., 2004).

During the interval from ~5.5 to 5 ka, an eolian sand layer in the TQ section occurs (Fig. 2), parallel decreases in  $\chi$  and  $\delta^{13}\text{C}_{\text{org}}$  and  $\text{C}_4$

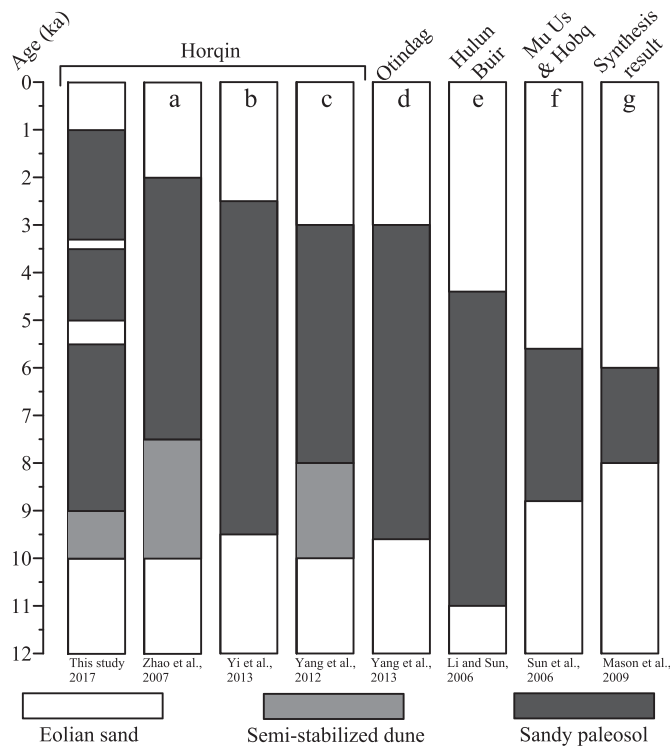


**Fig. 4.** Synthesis of intervals of paleosol formation based on OSL chronologies in the Horqin desert and adjacent deserts during the Holocene (see Fig. 1 for the location of each desert). The dating uncertainty of the plotted profiles is below 10% and has slight effect on the conclusion.

biomass in both sections (Figs. 2 and 3) indicate the remobilization of dunes and decreases in vegetation coverage and thus the termination of the Holocene climatic optimum. In eastern Inner Mongolia, a decrease in  $C_4$  biomass (Huang et al., 2005) and minima in precipitation and temperature (Jiang et al., 2006) occurred at ~5 ka. The shift to a colder climate was ascribed to decreased Northern Hemisphere summer insolation. In the Chinese Loess Plateau, a rapid increase in the accumulation rate of loess occurred at ~5 ka (Wang et al., 2014) and was ascribed to a ~5 ka weak EASM event (Wang et al., 2005). These findings suggest that at ~5 ka, a short-lived cold and dry event marked the termination of the Holocene climatic optimum.

Starting at ~5 ka and continuing to ~1 ka, a cold and dry climate is indicated by lower values of  $\chi$  and  $\delta^{13}C_{org}$  and  $C_4$  biomass in the TQ and MTG sections, and by the alternation of paleosol formation and eolian sand accumulation in the TQ section (Fig. 2). In the TQ section, the uppermost OSL date, with an age of ~0 ka, occurs at a depth of about 1.3 m. If this is correct, there has been a very rapid accumulation of sandy paleosols or blown sand in the recent past. However, there is no field evidence for such a rapid accumulation of sandy paleosols or blown sand in recent centuries. In fact, the shallowest sandy paleosol layer in the TQ section, mixed with modern soil, is the product of local human activity.

## 5.2. Regional comparison of climatic records

Studies carried out during the last two decades have improved our knowledge of paleoenvironmental changes in China, specifically of past shifts in the desert-grassland border in the deserts of the northeast (Fig. 1). Although this work does not fully constrain the timing of the changes, because of possible dating errors and discontinuous stratigraphic sequences in different geomorphic

units (Lu et al., 2011), overall its findings are in good agreement with our conclusions regarding the nature of environmental changes in the Horqin desert on a millennial time scale.

During the Holocene, paleosol records from the southeastern part (Fig. 4a), from the perimeter (Fig. 4b) and from the interior (Fig. 4c) of the Horqin desert, and from adjacent deserts (Fig. 4d and f), suggest that dune semi-stabilization occurred during the early Holocene; dune stabilization and paleosol development during the mid-Holocene; and the alternation of dune stabilization and mobilization during the late Holocene. This pattern was ascribed to changes in the insolation-driven strength of the EASM (Li and Sun, 2006; Sun et al., 2006; Zhao et al., 2007; Yang et al., 2010, 2013, 2012; Yi et al., 2013), while both climate and human land use played a role during the late Holocene (Zhao et al., 2007; Yang et al., 2012; Sun et al., 2006; Wang et al., 2008). The paleosol records described herein are in accordance with the findings of these studies and this similarity clearly demonstrates common forcing factors of environmental changes in these deserts during the Holocene.

Recently, however, the timing of the mid-Holocene interval of wettest climate along the margin of the EASM front has been disputed (Fig. 1). Palynological and ostracod data from Hulun Lake, spanning the interval from 8.3 to 6.2 ka, indicate that monsoon precipitation increased at this time (Wen et al., 2010; Zhai et al., 2011), in agreement with paleosol records from the Mu Us and Hobq deserts (Sun et al., 2006). To the west, in Inner Mongolia, the level of Daili Lake maintained a high stand from ~7.6 to 3.5 ka (Xiao et al., 2008); and in addition, a proxy MAP record from Bayanchagan Lake indicates that precipitation was up to 30–60% higher than today during the interval from ~10 to 6.5 ka, with a maximum in EASM precipitation of about 500 mm from ~7.9 to 6.9 ka. To the southwest, pollen assemblages and concentrations from Daihai Lake suggest a warm and humid climate from ~7.9 to 4.5 ka (Xiao et al., 2004), and grain-size records indicate intensified and highly variable monsoonal precipitation from ~7.9 to 3.1 ka in this region (Peng et al., 2005). In addition, pollen records from Gonghai Lake indicate that the wettest climate and strongest summer monsoon occurred from ~7.8 to 5.3 ka (Chen et al., 2015). In a more western location, at Qinghai Lake, an interval of warm and wet climate occurred from ~10 to 4 ka, with a maximum at ~6.5 ka (Shen et al., 2005). Further evidence for a strong EASM during the mid-Holocene is provided by a significant increase in the frequency of paleosol development from ~8.8 to 3.4 ka in the Chinese Loess Plateau (Wang et al., 2014). Furthermore, it is noteworthy that the Yangshao Culture attained its maximum development from ~7 to 5 ka in semiarid North China (IACASS, 2010). These results all support our finding that maximum EASM precipitation and paleosol development in the Horqin desert occurred during the mid-Holocene.

A significant conclusion from the foregoing is that maximum EASM precipitation exhibited a lagged response of about 5–2 ka to the peak in Northern Hemisphere summer insolation. There is an increasing amount of discussion of this issue (e.g. Imbrie and Imbrie, 1980; Xiao et al., 2004, 2008; Peng et al., 2005; Wen et al., 2010; Zhai et al., 2011; Chen et al., 2015). A possible explanation for this phenomenon (e.g. work of Xiao et al., 2004, 2008) is that the presence of remnant ice sheets in the Northern Hemisphere obstructed the northward retreat of the polar front in the North Pacific Ocean, and hampered the northward penetration of the summer monsoonal front, thereby suppressing monsoon precipitation over northern China. And a result, suggested by Chen et al. (2015), is that the remnant melting Laurentide ice sheet delivered continuous freshwater input to the North Atlantic and weakened the Atlantic Meridional Overturning Circulation (AMOC) (McManus et al., 2004), strongly offsetting the land-sea

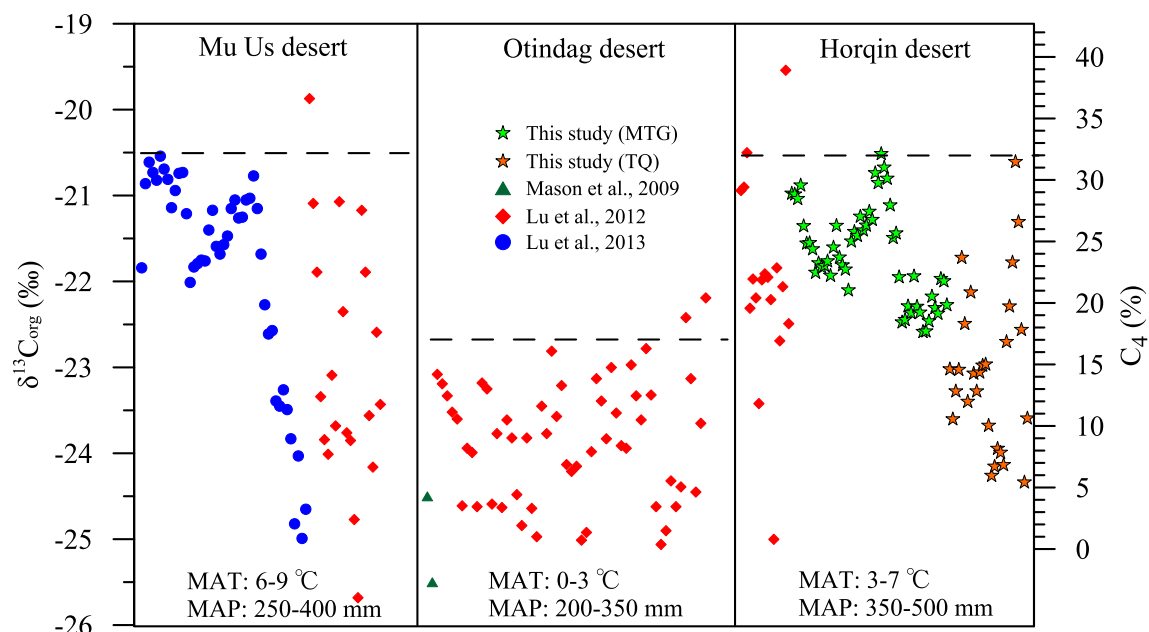


**Fig. 5.** Results of  $\delta^{13}\text{C}_{\text{org}}$  analyses and estimated  $\text{C}_4$  biomass for Holocene sediments from three deserts in northeastern China. Modern MAT and MAP in these deserts are also shown.

thermodynamic contrast and depressing the insolation-driven EASM. For this reason, we assume that the melting Laurentide ice sheet and the existence of other decaying ice sheets in the Northern Hemisphere jointly reduced EASM precipitation over northern China during the early Holocene and were responsible for the  $\sim 5\text{--}2$  ka lagged response to the peak in Northern Hemisphere summer insolation. This conclusion is supported by evidence for catastrophic iceberg discharge associated with the transient 8.2 ka climatic event (Alley and Ágústsson, 2005) which is recorded by stalagmite records in south China (Wang et al., 2005). However, it is important to note that dating uncertainties and discontinuous stratigraphic sequences in different geomorphic units may also be partially responsible for the inferred lag of EASM precipitation to Northern Hemisphere summer insolation. In addition, a global interpretation considered both northern and southern hemisphere influences during the last glacial cycle (Rohling et al., 2009).

After  $\sim 5$  ka, the alternation of dune stabilization and mobilization in the Horqin desert indicates significant fluctuations in EASM precipitation, presumably reflecting episodes of weakened EASM (Wang et al., 2005, 2010), as well as possible human activity (Sun et al., 2006; Wang et al., 2008). During the late Holocene, orbitally-induced insolation (Laskar et al., 2004) triggered the weakening of the EASM and decreases in sea surface temperatures in the low-latitude western tropical Pacific (Stott et al., 2004). This ocean-atmosphere thermodynamical effect reduced the moisture transported via the monsoon circulation from the western tropical Pacific into the interior of Asia and thus weakened the EASM (Xiao et al., 2002, 2004, 2008; Peng et al., 2005; Wen et al., 2010; Zhai et al., 2011). In addition, it is noteworthy that historical documents indicate that after 916 CE (the Liao dynasty to the present; Hu et al., 2002), people from Central China migrated to the Xiliao River drainage area and the resulting agricultural activity resulted in environmental deterioration and accelerated desertification. In addition, records of an anthropogenic influence on dune evolution in the Horqin desert during the last 3 ka come from a comparison of possible dune activation and evidence for human activity (Yang et al., 2012).

From the foregoing, it can be concluded that multiple factors

were responsible for the observed environmental changes in the Horqin desert during the Holocene. Based on our findings and previous studies, we conclude that the changes were strongly related to movement of the EASM rainfall belt during the Holocene, in response to changes in Northern Hemisphere summer insolation and low latitude ocean-atmosphere thermodynamical effects and Northern Hemisphere ice sheet effects, and that human land use also played a role during the late Holocene.

### 5.3. Significance of variations of $\text{C}_4$ biomass in the Horqin desert during the Holocene

An important question is why the values of  $\text{C}_4$  biomass in the MTG section are higher than those of the TQ section (Fig. 5). One possibility is that the effective moisture, an important limiting factor for the growth and distribution of plants (Mason et al., 2009), had a significant effect on the  $\text{C}_4$  biomass, since within the Horqin desert MAP ranges from 500 mm in the southeast to 350 mm in the northwest. Comparison of  $\delta^{13}\text{C}_{\text{org}}$  records from three deserts in northeastern China (Fig. 5) reveals that the  $\text{C}_4$  plant distribution was controlled by temperature and EASM precipitation (Lu et al., 2012).

Modern surveys have revealed that temperature and moisture conditions within the latitudinal range between  $31^\circ\text{N}$  and  $40^\circ\text{N}$  in eastern China favor the growth of  $\text{C}_4$  plants (Rao et al., 2008). However, phytolith records from eastern Inner Mongolia (Huang et al., 2005) reveal that between  $\sim 10$  ka and  $\sim 5$  ka  $\text{C}_4$  plants were dominant in a *Stipa grandis* steppe, in accordance with our  $\text{C}_4$  biomass records. Our vegetation records thus indicate that favorable growing conditions for  $\text{C}_4$  plants extended at least to the TQ section ( $45^\circ\text{N}$ ) during the early and middle Holocene. Consequently, it is possible to speculate that the ongoing global warming and the resulting northward movement of the EASM rainfall belt may, in the absence of any intensification of human land use, cause a regional reversal of the late Holocene aridification trend in the Horqin desert.

## 6. Conclusions

Paleosols in the Horqin desert on the margin of the EASM front have great potential for reconstructing past vegetation and climate changes during the Holocene. Our results reveal that the dunes in the region were semi-stabilized from ~11 to 9 ka, in response to gradually increasing EASM precipitation. From ~9 to 5 ka, extensive paleosol development occurred and C<sub>4</sub> biomass exhibited high values, indicating that formerly active dunes were largely fixed in response to intensified monsoonal precipitation. After ~5 ka, alternating eolian sand accumulation and paleosol development occurred. The C<sub>4</sub> biomass record clearly reveals that favorable growing conditions for C<sub>4</sub> plants extended to at least 45°N in North China during the early and middle Holocene.

Comparison of lake and paleosols record from the margin of the EASM reveals that Holocene environmental changes in the Horqin desert were controlled by the movement of the EASM rainfall belt in response to changes in Northern Hemisphere summer insolation. However, the maximum in EASM precipitation lagged the early Holocene maximum in Northern Hemisphere summer insolation by some 5–2 ka, possibly because of the thermodynamical effects of decaying Northern Hemisphere ice sheets in modulating EASM precipitation. During the late Holocene, intensive human land use, as well as the low latitude ocean-atmosphere system, may have had a significant influence on the environment of the Horqin desert. Nonetheless, it is clear that, overall, low latitude ocean-atmosphere thermodynamical effects and Northern Hemisphere ice sheet effects were the dominant influences on EASM precipitation over northern China during the Holocene, and ultimately modulated the Holocene environmental changes in the Horqin desert.

## Acknowledgments

We are grateful to the National Basic Research Program of China (grant 2013CB956403), the Strategic Priority Research Program of the Chinese Academy of Science (grant XDB03020503), and the National Nature Science Foundation of China (grant 41272206) for providing the funding. We thank Xu Wang and Linlin Cui for assistance in the laboratory, and Shiling Yang and Wenying Jiang and Zihua Tang for critical discussions, and Dr. Jan Bloemendal for improving an early version of the manuscript. We also thank C. Zeeden, and the other anonymous reviewer, and Slobodan Marković and Editor-in-Chief Prof. Min-Te Chen for their constructive comments and suggestions.

## Appendix A. Supplementary data

Supplementary data related to this article can be found at <http://dx.doi.org/10.1016/j.quaint.2017.06.048>.

## References

- Aitken, M.J., 1998. *An Introduction to Optical Dating*. Oxford University Press, Oxford, New York, Tokyo, pp. 43–44.
- Alley, R.B., Ágústsson, A.M., 2005. The 8k event: cause and consequences of a major Holocene abrupt climate change. *Quat. Sci. Rev.* 24, 1123–1149.
- An, Z.S., Huang, Y.S., Liu, W.G., Guo, Z.T., Clemens, S., Li, L., Prell, W., Ning, Y.F., Cai, Y.J., Zhou, W.J., Lin, B.H., Zhang, Q.L., Cao, Y.N., Qiang, X.K., Chang, H., Wu, Z.K., 2005. Multiple expansions of C<sub>4</sub> plant biomass in East Asia since 7 Ma coupled with strengthened monsoon circulation. *Geology* 33, 705–708.
- Chen, F.H., Xu, Q.H., Chen, J.H., Birks, H.J.B., Liu, J.B., Zhang, S.R., Jin, L.Y., An, C.B., Telford, R.J., Cao, X.Y., Wang, Z.L., Zhang, X.J., Selavraj, K., Lu, H.Y., Li, Y.C., Zheng, Z., Wang, H.P., Zhou, A.F., Dong, G.H., Zhang, J.W., Huang, X.Z., Bloemendal, J., Rao, Z.G., 2015. East Asian summer monsoon precipitation variability since the last deglaciation. *Sci. Rep.* <http://dx.doi.org/10.1038/srep11186>.
- Dong, G.R., Jin, J., Li, B.S., Gao, S.Y., Shao, Y.J., 1994. Several problems on the desertification of Horqin sandy land, Northeast China—a case study on its south area. *J. Desert Res.* 14, 1–9 (In Chinese with English abstract).
- Guo, L.C., Wu, J.B., Xiong, S.F., Yang, S.L., 2016. New sedimentary particles sorting process based on Hydrostatic Sedimentation Method. *J. Earth Sci. Environ.* 38, 694–699 (In Chinese with English abstract).
- Hu, J.M., Cui, H.T., Li, Y.Y., 2002. Reconstruction of the evolution history of man land system since the Holocene in the Xiliao River Basin. *Sci. Geogr. Sin.* 22, 535–541 (In Chinese with English abstract).
- Hu, M.C., 1989. The Holocene environmental changes in Keerqin sandy land. *J. Arid Land Resour. Environ.* 3, 51–58 (In Chinese with English abstract).
- Huang, F., Lias, K., Xiong, S.F., Huang, F.B., 2005. Holocene grassland vegetation, climate and human impact in central eastern Inner Mongolia. *Sci. China Ser. D Earth Sci.* 48, 1025–1039.
- IACASS (Institute of Archaeology Chinese Academy of Social Sciences), 2010. *Chinese Archaeology, Neolithic Volume*. China Social Science Press, Beijing (In Chinese).
- Imbrie, J., Imbrie, J.Z., 1980. Modeling the climatic response to orbital variations. *Science* 207, 943–953.
- Jiang, W.Y., Guo, Z.T., Sun, X.J., Wu, H.B., Chu, G.Q., Yuan, B.Y., Hatté, C., Guiot, J., 2006. Reconstruction of climate and vegetation changes of lake Bayanchagan (inner Mongolia): Holocene variability of the east Asian monsoon. *Quat. Res.* 65, 411–420.
- Kang, S.K., Wang, X.L., Lu, Y.C., Liu, W.G., Song, Y.G., Wang, N., 2015. A high-resolution quartz OSL chronology of the Taledo loess over the past ~30ka and its implications for dust accumulation in the Ili Basin, Central Asia. *Quat. Geochronol.* 30, 181–187.
- Laskar, J., Robutel, P., Joutel, F., Gastineau, M., Correia, A.C.M., Levrard, B., 2004. A long-term solution for the insolation quantities of the Earth. *Astron. Astrophys.* 428, 261–285.
- Li, Q., Wu, H.B., Guo, Z.T., Yu, Y.Y., Ge, J.Y., Wu, J.Y., Zhao, D.A., Sun, A.Z., 2014. Distribution and vegetation reconstruction of the deserts of northern China during the mid-Holocene. *Geophys. Res. Lett.* 41, 5184–5191.
- Li, S.H., Sun, J.M., 2006. Optical dating of Holocene dune sands from the Hulun Buir desert, northeastern China. *Holocene* 16, 457–462.
- Lu, H.Y., Mason, J.A., Stevens, T., Zhou, Y.L., Yi, S.W., Miao, X.D., 2011. Response of surface processes to climatic change in the dune fields and Loess Plateau of North China during the late Quaternary. *Earth Surf. Process. Landforms* 36, 1590–1603.
- Lu, H.Y., Yi, S.W., Liu, Z.Y., Mason, J.A., Jiang, D.B., Cheng, J., Stevens, T., Xu, Z.W., Zhang, E.L., Jin, L.Y., Zhang, Z.H., Guo, Z.T., Wang, Y., Otto-Bliesner, B., 2013. Variation of East Asian monsoon precipitation during the past 21 k.y. and potential CO<sub>2</sub> forcing. *Geology* 41, 1023–1026.
- Lu, H.Y., Zhou, Y.L., Liu, W.G., Mason, J.A., 2012. Organic stable carbon isotopic composition reveals late Quaternary vegetation changes in the dune fields of northern China. *Quat. Res.* 77, 433–444.
- Maher, B.A., Thompson, R., 1995. Paleorainfall reconstructions from pedogenic magnetic susceptibility variations in the Chinese loess and paleosols. *Quat. Res.* 44, 383–391.
- Mason, J.A., Lu, H.Y., Zhou, Y.L., Miao, X., Swinehart, J.B., Liu, Z.Y., Goble, R.J., Yi, S.W., 2009. Dune mobility and aridity at the desert margin of northern China at a time of peak monsoon strength. *Geology* 37, 947–950.
- McManus, J.F., Francois, R., Gherardi, J.M., Keigwin, L.D., Brown-Leger, S., 2004. Collapse and rapid resumption of Atlantic meridional circulation linked to deglacial climate changes. *Nature* 428, 834–837.
- Meng, X., Derbyshire, E., Kemp, R.A., 1997. Origin of the magnetic susceptibility signal in Chinese loess. *Quat. Sci. Rev.* 16, 833–839.
- Peng, Y.J., Xiao, J.L., Nakamura, T., Liu, B.L., Inouchi, Y., 2005. Holocene East Asian monsoonal precipitation pattern revealed by grain-size distribution of core sediments of Daihai Lake in Inner Mongolia of north-central China. *Earth Planet. Sci. Lett.* 233, 467–479.
- Prescott, J.R., Hutton, J.T., 1994. Cosmic-ray contributions to dose-rates for luminescence and ESR dating: large depths and long-term time variations. *Radiat. Meas.* 23, 497–500.
- Qiu, S.W., Li, Q.S., Xia, Y.M., 1992. Paleosols of sandy lands and environmental changes in the western plain of Northeast China during Holocene. *Quat. Sci.* 3, 224–232 (In Chinese with English abstract).
- Rao, Z.G., Jia, G.D., Zhu, Z.Y., Wu, Y., Zhang, J.W., 2008. Comparison of the carbon isotope composition of total organic carbon and long-chain n-alkanes from surface soils in eastern China and their significance. *Chin. Sci. Bull.* 53, 3921–3927.
- Ren, G.Y., 1999. Influence of human activities on the late Holocene vegetation changes at Maili, northeast China. *Sci. Geogr. Sin.* 19, 42–48 (In Chinese with English abstract).
- Ren, H.C., Lü, Y.L., Yang, P., Chen, H.Z., Shi, Y.J., 2004. History and present status of desertification in Horqin sandy land region. *J. Desert Res.* 24, 544–547 (In Chinese with English abstract).
- Ren, M.E., Yang, R.Z., Bao, H.S., 1985. *An Outline of China's Physical Geography*. Foreign Languages Press, Beijing, pp. 346–361.
- Rohling, E.J., Liu, Q.S., Roberts, A.P., Stanford, J.D., Rasmussen, S.O., Langen, P.L., Siddall, M., 2009. Controls on the East Asian monsoon during the last glacial cycle, based on comparison between Hulu Cave and polar ice-core records. *Quat. Sci. Rev.* 28, 3291–3302.
- Shen, J., Liu, X.Q., Wang, S.M., Matsumoto, R., 2005. Palaeoclimatic changes in the Qinghai Lake area during the last 18,000 years. *Quat. Int.* 136, 131–140.
- Stott, L., Cannariato, K., Thunell, R., Haug, G.H., Koutavas, A., Lund, S., 2004. Decline

- of surface temperature and salinity in the western tropical Pacific Ocean in the Holocene epoch. *Nature* 431, 56–59.
- Sun, J.M., Li, S.H., Han, P., Chen, Y.Y., 2006. Holocene environmental changes in the central Inner Mongolia, based on single-aliquot-quartz optical dating and multi-proxy study of dune sands. *Palaeogeogr. Palaeoclimatol. Palaeoecol.* 233, 51–62.
- Wang, G.A., Feng, X.H., 2012. Response of plants' water use efficiency to increasing atmospheric CO<sub>2</sub> concentration. *Environ. Sci. Technol.* 46, 8610–8620.
- Wang, G.A., Li, J.Z., Liu, X.Z., Li, X.Y., 2013. Variations in carbon isotope ratios of plants across a temperature gradient along the 400 mm isohet of annual precipitation in north China and relevance to paleovegetation reconstruction. *Quat. Sci. Rev.* 63, 83–90.
- Wang, H.P., Chen, J.H., Zhang, X.J., Chen, F.H., 2014. Palaeosol development in the Chinese Loess Plateau as an indicator of the strength of the East Asian summer monsoon: evidence for a mid-Holocene maximum. *Quat. Int.* 334, 155–164.
- Wang, X.M., Chen, F.H., Hasi, E., Li, J.C., 2008. Desertification in China: an assessment. *Earth Sci. Rev.* 88, 188–206.
- Wang, Y.B., Liu, X.Q., Herzschuh, U., 2010. Asynchronous evolution of the Indian and East Asian summer monsoon indicated by Holocene moisture patterns in monsoonal central Asia. *Earth Sci. Rev.* 103, 135–153.
- Wang, Y.J., Cheng, H., Edwards, R.L., He, Y.Q., Kong, X.G., An, Z.S., Wu, J.Y., Kelly, M.J., Dykoski, C.A., Li, X.D., 2005. The Holocene Asian monsoon: links to solar changes and North Atlantic climate. *Science* 308, 854–857.
- Wen, R.L., Xiao, J.L., Chang, Z.G., Zhai, D.Y., Xu, Q.H., Li, Y.C., 2010. Holocene climate changes in the mid-high-latitude-monsoon margin reflected by the pollen record from Hulun Lake, northeastern Inner Mongolia. *Quat. Res.* 73, 293–303.
- Wintle, A.G., Murray, A.S., 2006. A review of quartz optically stimulated luminescence characteristics and their relevance in single-aliquot regeneration dating protocols. *Radiat. Meas.* 41, 369–391.
- Xiao, J.L., Nakamura, T., Lu, H.Y., Zhang, G.Y., 2002. Holocene climate changes over the desert/loess transition of north-central China. *Earth Planet. Sci. Lett.* 197, 11–18.
- Xiao, J.L., Si, B., Zhai, D.Y., Itoh, S., Lomtatidze, Z., 2008. Hydrology of Dali Lake in central-eastern inner Mongolia and Holocene East Asian monsoon variability. *J. Paleolimnol.* 40, 519–528.
- Xiao, J.L., Xu, Q.H., Nakamura, T., Yang, X.L., Liang, W.D., Inouchi, Y., 2004. Holocene vegetation variation in the Daihai Lake region of north-central China: a direct indication of the Asian monsoon climatic history. *Quat. Sci. Rev.* 23, 1669–1679.
- Xiong, S.F., Ding, Z.L., Liu, T.S., Zhang, J.Z., 2002. East Asian monsoon instability at the stage 5a/4 transition. *Boreas* 31, 126–132.
- Xu, Z.W., Lu, H.Y., Yi, S.W., Vandenberghe, J., Mason, J.A., Zhou, Y.L., Wang, X.Y., 2015. Climate-driven changes to dune activity during the Last Glacial Maximum and deglaciation in the Mu Us dune field, north-central China. *Earth Planet. Sci. Lett.* 427, 149–159.
- Yang, L.H., Wang, T., Zhou, J., Lai, Z.P., Long, H., 2012. OSL chronology and possible forcing mechanisms of dune evolution in the Horqin dunefield in northern China since the Last Glacial Maximum. *Quat. Res.* 78, 185–196.
- Yang, L.H., Zhou, J., Lai, Z.P., Long, H., Zhang, J.R., 2010. Lateglacial and Holocene dune evolution in the Horqin dunefield of northeastern China based on luminescence dating. *Palaeogeogr. Palaeoclimatol. Palaeoecol.* 296, 44–51.
- Yang, S.L., Ding, Z.L., Li, Y.Y., Wang, X., Jiang, W.Y., Huang, X.F., 2015b. Warming-induced northwestward migration of the East Asian monsoon rain belt from the Last Glacial Maximum to the mid-Holocene. *Proc. Natl. Acad. Sci. U. S. A.* 112, 13178–13183.
- Yang, X.P., Scuderi, L.A., Wang, X.L., Scuderi, L.J., Zhang, D.G., Li, H.W., Forman, S., Xu, Q.H., Wang, R.C., Huang, W.W., Yang, S.X., 2015a. Groundwater sapping as the cause of irreversible desertification of Hunshandake Sandy Lands, Inner Mongolia, northern China. *Proc. Natl. Acad. Sci. U. S. A.* 112, 702–706.
- Yang, X.P., Wang, X.L., Liu, Z.T., Li, H.W., Ren, X.Z., Zhang, D.G., Ma, Z.B., Rioual, P., Jin, X.D., Scuderi, L., 2013. Initiation and variation of the dune fields in semi-arid northern China—with a special reference to the Hunshandake Sandy Land, Inner Mongolia. *Quat. Sci. Rev.* 78, 369–380.
- Yi, S.W., Lu, H.Y., Zeng, L., Xu, Z.W., 2013. Paleoclimate changes and reconstruction of the border of Horqin dunefield (northeastern China) since the last glacial maximum. *Quat. Sci.* 33, 206–217 (In Chinese with English abstract).
- Zhai, D.Y., Xiao, J.L., Zhou, L., Wen, R.L., Chang, Z.G., Wang, X., Jin, X.D., 2011. Holocene East Asian monsoon variation inferred from species assemblage and shell chemistry of the ostracodes from Hulun Lake, Inner Mongolia. *Quat. Res.* 75, 512–522.
- Zhao, H., Lu, Y.C., Yin, J.H., 2007. Optical dating of Holocene sand dune activities in the Horqin sand-fields in Inner Mongolia, China, using the SAR protocol. *Quat. Geochronol.* 2, 29–33.